Research Report for the Austrian Marshall Plan Foundation

The Utility of 3D Laser Scanning in the Fatigue Assessment of Welds

by Alexander Niederwanger

Supervision:
Univ.-Prof. Dr. Gerhard Lener
Department of Structural Engineering and Material Scienes
University of Innsbruck, 6020 Innsbruck, Austria

and

Prof. Derek H. Warner, PhD
Cornell Fracture Group, School of Civil and Environmental Engineering
Cornell University, Ithaca, NY 14853, United States

Innsbruck, January 2020

Table of Contents

1 Introduction

Fatigue is known as the phenomenon of cracks occurring in a cyclically loaded component or structure. The fatigue strength of a material is often much lower than its static strength. In high cycle fatigue, for instance, cracks may initiate at stresses way below the material's yield stress. Once a crack is initiated, it propagates a small amount of distance with every loading cycle until the component fails. If such a damaged component is crucial for the whole structure, a fatigue crack could ultimately lead to the failure of that structure or building. A very prominent example from everyday life is the paper clip. Imagine bending a straightened paper clip to the left, then to the right, and finally back to its original position. This bending operation is considered as one loading cycle. While probably nothing except some major deformation can be observed after one loading cycle, the paper clip starts to fatigue and fail eventually after some more. Due to the large plastic deformations that the material experiences, the number of cycles to failure may be very low, probably below ten. Such a case is classified as low cycle fatigue (LCF). Depending on the source consulted, low cycle fatigue goes up to around 1000 loading cycles. High cycle fatigue (HCF), on the other hand, refers to fatigue failure that occurs up to approximately 1e6 cycles. Again, the terminology depends on the respective literature and may vary up to one magnitude in each direction. Fatigue damage beyond those points is referred to as very high cycle fatigue (VHCF). The present work primarily deals with the phenomenon of high cycle fatigue as the specimens in the conducted experiments were subjected to a number of loading cycles between 50,000 and 1e6.

History books report many severe disasters and catastrophes, many of which are due to material fatigue. In 1943, for instance, the SS Schenectady, a United States tanker, cracked almost in half in calm waters shortly after completing sea trials. Many other ships of the same construction series, they are also referred to as the Liberty ships, sunk during World War II. A lot of those failures could be traced back to fatigue damage. Due to the immense increase in production capacity at that time, the quality decreased significantly. Investigations revealed that defective welding in combination with low-grade steel was the most common reason why these ships failed and sunk eventually [1, 2].

Another inglorious example of metal fatigue is the crash of two Comet airplanes in the 1950s. The Comet 1 was the world's first commercial jet airliner and flew the first time in 1949. After only a few years in service, two Comet aircraft crashed shortly after each other. Investigations confirmed that the unfavorable squared shape of the windows caused high stress concentrations at the corners, which resulted in fatigue crack initiating from those regions. These two accidents influenced the shape of the windows as they are now in modern aircraft constructions. Due to the smoother shape and larger radii at the corners, fewer stress concentrations are caused, which results in safer fatigue design. However, this is no guarantee that fatigue cracks will never occur, which is why inspections in regular intervals are mandatory [3].

The problem of metal fatigue is not only limited to ships and airplanes. Fatigue cracks may also initiate in other structures, such as steel bridges, cars, trucks, cranes, or even bicycles. Basically, any component that is subjected to cyclic loading may experience fatigue damage and eventually fail if the number of loading cycles is high enough. At this point, it should be noted that the question of an ultimate fatigue limit is a current state of research and still debated in the scientific community. Since this question is not part of the present work, the interested reader is referred to the literature, e.g., [4, 5].

1.1 Fatigue Crack Initiation

Fatigue cracks usually initiate at locations of high stress concentrations. Most of the time, those stress concentrations are caused by inconsistencies in the geometry of a structure. For instance, a hole that is cut out of a steel plate forces the stress trajectories to bend around the hole, which results in high stress concentrations at the edge of that hole. Such stress raisers are usually referred to as notches. The sharper the notch, i.e., the smaller the radius of the cut-out hole in the previous example, the higher the stress concentrations, which results in earlier fatigue failure. The surface of a weld is also a good example of a notch. The smoother the transition between the weld and the base material, the larger is the notch radius, which is beneficial regarding the fatigue behavior of the weld. Generally speaking, the sharper a notch in a material is, the higher are the stress concentrations in the vicinity of the notch, and the lower is the fatigue life of that component. Notches also occur at locations where one might not expect them at first sight. For example, two bodies that are pressed against each other cause stress concentrations at and near the contact area. The magnitude of the stresses in that region depends on the stiffness of both bodies.

If a meterial is repeatedly loaded and unloaded, irreversible slips at the microscopic scale are induced. With every loading cycle, those localized slips accumulate until material separation follows eventually. This phenomenon is known as fatigue crack formation at the microlevel. After the nucleation, the crack grows and propagates incrementally through the microstructure of the material. Generally, the crack growth behavior in ductile materials can be divided into two stages, the micro-sensitive stage (also referred to as stage I) and the microstructure-independent stage II. In the first stage, crack growth is governed by combined opening and sliding mechanisms (mode I and mode II/III) and evolves along with the slip with the maximum shear stress. Those directions may vary from grain to grain, as illustrated in the left part of Fig. 1. Crack growth in the second stage is independent of the grains and is primarily controlled by the opening mode. In this stage, the crack advances until the final rupture, [6].

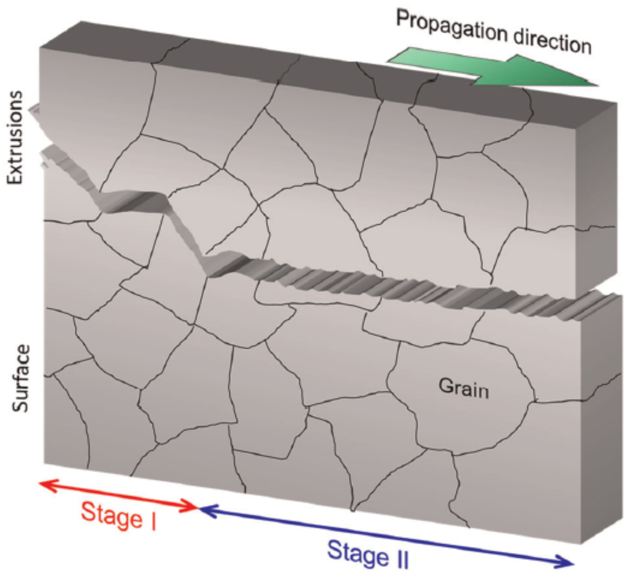

Fig. 1: Stage I and stage II fatigue crack growth. Image taken from [6].

1.2 Fatigue Assessment

Over the years, many different approaches and models have been developed to design a component or structure against fatigue failure. Some are more sophisticated from a theoretical point of view, whereas other models are easier to apply for the design engineer and require less detailed knowledge of the underlying processes and damage mechanisms. In the following, three frequently used design concepts, which are also part of state-of-the-art standards and guidelines, such as the Eurocode [7], the IIW recommendations [8], or the FKM recommendations [9], are briefly presented. All of the models discussed in the present work can be described by straight lines in a logarithmic plot, which are known as stress-life curves or Wöhler curves, based on the works of the German railway engineer August Wöhler.

1.2.1 Nominal Stress Concept

The nominal stress approach is somewhat simple to apply, since only far-field stresses, so-called nominal stresses, are required to predict the fatigue life of a component. Those stresses can either be determined analytically or, if the geometry of the structure gets more complicated, using numerical methods, such as a finite element analysis (FEA). The obtained stress range values are then compared to fatigue classes, which describe the bearable stress range at 2e6 loading cycles. Many different fatigue classes, based on a large number of experiments, are defined in the previously mentioned guidelines. The design engineer has to choose the proper detail in order to obtain the correct fatigue resistance. Once both the fatigue class and the nominal stress range are determined, one can predict the fatigue life of the assessed structure.

1.2.2 Hot Spot Stress Concept

The idea behind the hot spot stress approach, which is also known as the structural stress approach and was developed for the assessment of welded joints, is similar to the nominal stress concept. The structural stress is defined as the stress caused by the macro-geometrical shape of a component, neglecting any local stress raisers, such as notches. The stress value in the critical fatigue region, the so-called hot spot, is determined by taking stress values a given distance away from that hot spot, and subsequently extrapolating those values to the hot spot. By doing so, the influence of the local geometry of the notch is not taken into account. Depending on the assessed detail, different recommendations regarding the extrapolation exist. The number of fatigue classes reduces significantly compared to the previously described approach. Once the fatigue class is determined, the assessment works identically. One drawback of the hot spot stress concept is that the root crack of a fillet weld cannot be assessed. However, attempts to overcome this issue exist [10].

1.2.3 Effective Notch Stress Concept

Within the notch stress approach, the number of fatigue classes reduces to one. Every notch in the model has to be rounded with a fictitious notch radius of 1 mm. By doing so, stress gradients perpendicular to the surface are taken into account. According to Neuber's micro support theory [11], a notch radius of 1 mm is equivalent to averaging stresses in a small material volume with the size of the micro support length, which is a material-dependent parameter. After calculating the maximum stress value at the notch, rounded with the fictitious radius of 1 mm, the fatigue life of the component can be determined as described before. The effective notch stress approach is able to consider fatigue crack initiation at the weld root, as opposed to the hot spot stress approach. Additionally, the fatigue resistance of the base material has to be assessed with the nominal stress approach, since the fatigue resistance of the effective notch stress approach is too high for base material.

All of the presented fatigue assessment approaches are based on linear elastic stress calculations. Other methods, e.g., the strain-life concept, exist, but since contribution at hand focuses on linear elastic stress calculations, those other concepts are not covered in this report.

2 Project Outline

The present work focuses on the fatigue behavior of welded joints. Different fatigue models, based on linear elastic stress computations, are fitted to experimental results and evaluated based on their ability to predict fatigue lives. In particular, the effects of using 3D laser scan technology to obtain an actual representation of the weld geometry on the accuracy of the fatigue life predictions are discussed.

The following content is taken from the research paper [12] that emerged from the collaboration between Cornell University and the University of Innsbruck during my research visit in the course of the Marshallplan scholarship. The manuscript has been submitted to the International Journal of Fatigue, where it is currently under review.

3 Literature Review

Over the last decade, the use of 3D laser scan technology in fatigue assessment has become increasingly popular. Not only notches and the stress concentration they cause can be captured, but also the stiffness of the investigated joint can be represented more accurately. However, scanning fatigue hot spots does not only have advantages; the required effort is not negligible. Scanning the specimen and post-processing the scanned data in order to obtain solids that can be used in a finite element (FE) computation is time-consuming. Depending on the assessed detail, a finer mesh is usually required to accurately capture the scanned surface, which leads to additional computation costs compared to using an idealized model.

The present work focuses on the fatigue assessment of welded joints, and the advantages of incorporating laser scan technology. The influence of the weld shape on the stress distribution and the fatigue life of a component is repeatedly reported in the literature, e.g., [13–17]. Whereas conventional approaches attempt to describe the weld geometry through the weld flank angle and the weld toe radius, newer concepts are based on scanned geometries.

Hou [18] was a pioneer at using laser scan technology in the fatigue assessment of welded components. He investigated fillet welds of non-load carrying cruciform joints. The scanned data was used to obtain a 3D representation of the weld for the FE model. Hou concluded that the locations of crack initiation correlated well with the calculated regions of plasticity. The final fracture of the specimen did not necessarily emerge from the weld with the highest stress concentration factor (SCF). Additionally, more than 10,000 SCF values were evaluated along the welds and found to follow a log-normal distribution.

Alam et al. [14] measured weld surface topographies of laser hybrid welded eccentric fillet joints. Based on 2D cuts derived from the scanned data and a subsequently performed FEA, they concluded that the weld toe radii and, therefore, the SCFs vary considerably along the weld. However, toe radii were not always dominating fatigue performance as ripples became local stress raisers in some cases.

Kaffenberger et al. [19, 20] investigated 3D scanned weld ends of overlap joints and T-joints. Based on linear elastic stress calculations, they derived recommendations on how to model an idealized weld geometry that can be used to assess these types of joints within the framework of the notch stress concept.

Lang E. et al. [15, 21] as well as Bosch et al. [22] incorporated scanned butt-welded joints in combination with local hardness measurements into their strain-life fatigue predictions. Based on their calculations, they derived local strain-life curves. They were able to predict the correct location of crack initiation (base material or weld toe) for the conducted low cycle fatigue experiments.

Stasiuk et al. [23] calculated stress concentrations at non-load carrying cruciform joints. Their FE computations were based on real three-dimensional weld geometries obtained through laser scanning. However, poor correlation between the predicted fatigue lives and the experimentally determined ones was observed.

Lang R. et al. [24, 25] statistically evaluated the shapes of welds manufactured in different welding techniques and positions. Additionally, the deformation of the specimens due to the welding process was measured. Based on their developed fatigue model, which is detailly described in [26], they also derived fatigue life curves for the assessed specimens.

Liinalampi et al. [27] investigated the fatigue behavior of 3 mm thick laser-hybrid welded butt joints. A large amount of scattering in the experimental results could be explained by the notch stress approach in combination with stresses obtained from real representations of the welds and Neuber's micro support theory [11]. In another work [16], they investigated weld undercuts and derived a 3D correction factor, which describes the ratio between the maximum effective notch stress in a 3D analysis compared to a 2D computation.

Ladinek et al. [28] applied the strain-life concept to 3D scanned weld geometries. A considerable amount of scatter in the predicted fatigue lives was observed applying different material data sets (all for the same base material) from the literature. A significant improvement regarding the prediction accuracy of the model was achieved by linking the material properties to local hardness measurements [29].

Schork et al. [17] performed line scans of welds of different joint types and steel grades to derive statistical distributions of weld parameters, such as weld toe radius, flank angle, excess metal height, and secondary notches. Material defects and non-metallic inclusions were analyzed by micro sectioning and fractography. The effects of these measured weld parameters and observed defects on the components' fatigue lives were investigated.

Stenberg et al. [30, 31] developed a tool based on laser scan technology to evaluate weld quality regarding different aspects, such as weld radius, undercut, throat thickness, or transition radius. In another study [32], they assessed fatigue lives of fillet welds of cruciform joints manufactured in standard and high-strength steel. Different sensitivities with respect to weld quality were reported for different steel grades.

Chaudhuri et al. [33] captured the real weld toe geometry, including inherent flaws, of non-load carrying cruciform joints using X-ray micro-computed tomography. The statistically evaluated stress concentration factors along the weld allowed an improved fatigue assessment.

The insights gained from laser scanning technology into the fatigue behavior of welded joints are manifold and certainly valuable. However, the question arises as to whether incorporating 3D scans of welds into the assessment approach leads to more accurate fatigue life predictions. The contribution at hand attempts to answer this question. After the Introduction, the different investigated fatigue models are described briefly in Section 2. Section 3 focuses on the tested fatigue specimens, the scanning process, and the numerical implementation. The results are discussed in Section 4 before conclusions are drawn, and the prospect for further research is given.

4 Investigated Approaches

Fatigue models are often defined on a logarithmic scale, linking stress values, or fatigue indicator parameters, in general, to the loading cycles up to crack initiation. In the present contribution, two-parameter Wöhler curves are fitted to experimental results by minimizing the root-mean-square error (RMSE) with respect to fatigue life. Mathematically, the model is expressed via

$$\log_{10} N_\mathrm{f} = \mathcal{A} \log_{10} X + \mathcal{B}, \tag{1}$$

which describes a straight line in a $\log_{10}$-$\log_{10}$ plot. The parameters $\mathcal{A}$ and $\mathcal{B}$ are the inverse slope of the curve and the intercept on the x-axis, respectively. N_f is the estimated cycles, and X denotes the value of the fatigue indicator parameter.

4.1 Fatigue Indicators

In total, six different fatigue indicator parameters, such as the signed von Mises equivalent stress

$$\sigma_\Sigma = \mathrm{sgn}(\sigma_1 + \sigma_3)\sigma_\mathrm{eq}, \tag{2}$$

the maximum principal stress σ_1, or the maximum shear stress τ_max, were used independently to predict fatigue lives.

Additionally, two damage parameters based on the critical-plane approach, namely the one by Findley [34, 35] (expressed in terms of strain)

$$P_\mathrm{CP} = \frac{\Delta\gamma}{2} + k\frac{\sigma_\mathrm{n}}{E}, \tag{3}$$

and the modification by Fatemi and Socie [36]

$$P_\mathrm{FS} = \frac{\Delta\gamma}{2}\left(1 + k\frac{\sigma_\mathrm{n}}{S_\mathrm{y}}\right), \tag{4}$$

are investigated. The material parameter k indicates the influence of the normal stress on fatigue damage and is set to one if no information is available, as recommended by Stephens et al. [37]. In the present work, stress tensors are rotated in increments of 1° to determine the critical plane, which yields the maximum damage parameter.

The strain energy density release rate Y according to Lemaitre [38] is also considered.

$$Y = \frac{\sigma_{\mathrm{eq}}^2}{2E} R_\nu, \tag{5}$$

with the triaxiality function

$$R_\nu = \frac{2}{3}(1+\nu) + 3(1-2\nu)\left(\frac{\sigma_{\mathrm{H}}}{\sigma_{\mathrm{eq}}}\right)^2. \tag{6}$$

σ_{H} denotes the hydrostatic part of the stress tensor.

For each of the six fatigue indicator parameters, three types of fatigue models, namely two deterministic ones (local and nonlocal) and one probabilistic model, are investigated and evaluated regarding their ability to accurately predict fatigue performance. Particular emphasis is given to whether incorporating scanned weld geometries in the models results in more reliable fatigue life predictions. For the nonlocal and the probabilistic approach, the difference between considering nonlocal effects through the volume or the surface area is additionally investigated. In total, 60 models are fitted to the experimental results and evaluated.

4.2 Local Model

Inspired by state-of-the-art codes and guidelines, such as the Eurocode [7] or the IIW recommendations [8], the maximum value of the fatigue indicator parameter in the specimen is assumed to govern fatigue crack initiation. Linear Wöhler curves, as described by Eq. (1), are fitted to the experimental results. Since only the maximum fatigue indicator is used to predict fatigue lives, i.e., not considering any nonlocal effects, they are referred to in the following as local or peak stress models.

4.3 Nonlocal Model

The nonlocal model is explained based on the example of the von Mises stress, but its application to the other fatigue indicator parameters is equivalent. It is commonly known [39–43] that a component's fatigue life is influenced not only by the maximum stress value at the notch but also by the stress distribution in the vicinity of the notch. Slight stress gradients lead to large regions that are subjected to stress values close to the maximum value, which is detrimental to fatigue life. Steep gradients, on the other hand, result in smaller highly stressed regions, which is less detrimental for a component's fatigue life. A possible method to account for these so-called size effects is the definition of a support factor n_{supp} based on the highly stressed region. Dividing the peak stress value by the support factor yields the effective stress

$$\sigma_{\mathrm{eff}} = \frac{\sigma_{\max}}{n_{\mathrm{supp}}}, \tag{7}$$

which is used to fit the Wöhler curve described by Eq. (1) and subsequently predict fatigue lives.

The literature provides different recommendations regarding the determination of the size of this highly stressed region. Whereas some define the contribution limit at 95% of the maximum stress value [44], others recommend values of 90% [41, 42] or 80% [43]. In the present paper, the highly stressed area is determined according to Liu et al. [45].

$$A_{\mathrm{HS}} = \int_A \left(\frac{\sigma(x,y,z)}{\sigma_{\max}} \right)^{\kappa} \mathrm{d}A \tag{8}$$

The Weibull exponent κ is material-dependent and reflects the scatter of the fatigue strength. The support factor n_{supp} follows to

$$n_{\mathrm{supp}} = \left(\frac{A_{\mathrm{ref}}}{A_{\mathrm{HS}}} \right)^{1/\kappa}, \tag{9}$$

where A_{ref} is the reference area, which is set to 1 mm^2 in the present work. For other values of the reference area, the intercept of the fitted Wöhler curve $\mathcal{B}$ changes, but its slope $\mathcal{A}$ and the Weibull exponent κ are unaffected. The definition of the highly stressed region in terms of volume is also frequently reported in the literature, e.g., [39, 41, 42], and, therefore, also investigated. This is accomplished by replacing the surface area in Eqs. (8) and (9) with the volume of the specimen. The reference volume is set to 1 mm^3.

4.4 Probabilistic Model

Despite modeling the real weld geometry and considering size effects through a highly stressed region, deterministic models might not be able to explain all the scatter observed in the experiments since other sources of uncertainty, such as defects, inclusions, grain size, or different material zones, are not taken into account. Therefore, a probabilistic model, originally proposed by Li et al. [46], is introduced to provide information on how the varying microstructure affects the fatigue life of a component. The two primary assumptions of the model are that fatigue failure can be mapped to a single crack initiation location, which is independently scattered throughout the specimen, and that the failure of a component is described by Weibull's weakest link model [47]. The latter implies that the survival probability of a specimen is the product of the survival probabilities of its subvolumes. The probability of survival S_i of each subvolume is assumed to follow a three-parameter Weibull distribution and is expressed through

$$S_i = P\left(\log_{10} N_{\mathrm{f}} \geq \log_{10} n_{\mathrm{f}}\right) = \exp\left(- \left(\frac{\log_{10} n_{\mathrm{f}} - \theta_i}{\lambda} \right)^{\beta} \right), \tag{10}$$

where N_{f} represents the number of cycles to failure and n_{f} is a given number of cycles for which the survival probability is calculated. The parameters β and λ are assumed to be independent of the fatigue indicator X and control the evolution of the failure rate with respect to $\log_{10} n_{\mathrm{f}}$ and the variance of $\log_{10} N_{\mathrm{f}}$, respectively. The location parameter θ corresponds to the minimum observable value of $\log_{10} N_{\mathrm{f}}$. Based on Eq. (1), the stress dependence of S_i is assumed to follow

$$\theta_i = \min\left(\mathcal{A} \log_{10} X_i + \mathcal{B} - \lambda (\ln 2)^{1/\beta},\ \log_{10} n_{\mathrm{f}} \right), \tag{11}$$

with

$$\mathrm{median}\left(\log_{10} N_{\mathrm{f}}\right) = \mathcal{A} \log_{10} X_i + \mathcal{B}. \tag{12}$$

The offset term $\lambda(\ln 2)^{1/\beta}$ in Eq. (11) aligns the median of the Wöhler curve with the median of the Weibull distribution.

The survival probability S of the specimen is calculated as the joint probability of its partitioning subvolumes, namely the volumes associated with each of the element nodes.

$$S = P\left(\log_{10} N_{\mathrm{f}} \geq \log_{10} n_{\mathrm{f}}\right) = \exp\left(\text{-}z\lambda^{-\beta} \int_V \left(\log_{10} n_{\mathrm{f}} - \theta\right)^{\beta} \mathrm{d}V\right) \tag{13}$$

The volume integral $\int_V$ can also be replaced by an area intregal, taking into account the stress distribution on the surface of the specimen only. The parameter z is interpreted as the inverse of the reference area or volume, and is set to $1/\mathrm{mm}^2$ and $1/\mathrm{mm}^3$, respectively. For other reference sizes, the value of the scale parameter λ changes to

$$\lambda_{\mathrm{new}} = \lambda_{\mathrm{ref}} \left(\frac{z_{\mathrm{new}}}{z_{\mathrm{ref}}}\right)^{1/\beta}. \tag{14}$$

The shape parameter β is unaffected by the choice of the reference size.

5 Specimens and Numerical Implementation

In total, 28 specimens from three different test series are investigated in the present study. All of them were manufactured in S355 mild steel and had similar static material properties. The applied load ratios in the experiments varied from around 0 to 0.1. Figure 2 provides an overview of the different specimen geometries and experimental set-ups. The critical fatigue spots are highlighted. Failure was defined as a surface crack visible to the human eye, which resulted in crack lengths of approximately 1 mm. The fatigue lives observed in the experiments range from about 50,000 to 1e6 cycles. A more detailed description of the experiments, containing applied loads, load ratios, and cycles at crack initiation of each specimen, can be found in Niederwanger et al. [48].

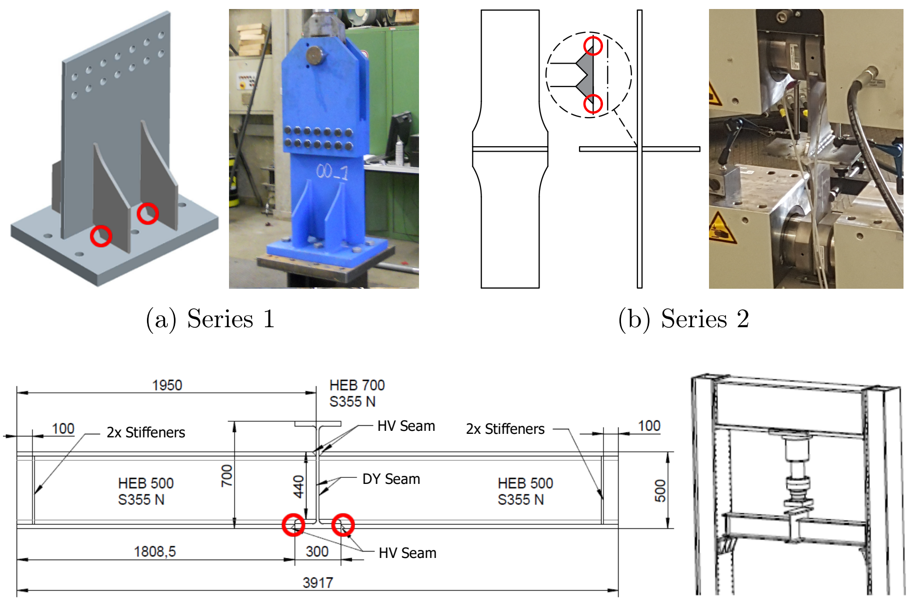

(a) Series 1

(b) Series 2

(c) Series 3

Fig. 2: Overview of the three test series, including specimen geometry and experimental set-up. Red circles indicate the fatigue critical spots. Images taken from [48].

Figure 3 illustrates the different notch geometries assessed in the present study at the example of von Mises stress plots. The screenshots highlight that the weld geometry significantly influences the stress distribution at the notch and, thus, the size of the highly stressed region. Fig. 3a presents two extreme cases of test series 2. The highly stressed region in the left plot is considerably larger than the one of the right specimen. The right plot in Fig. 3a shows a weld of test series 3, where the stress gradients are steep and, thus, the highly stressed area is very concentrated in a single spot. In the left picture, on the other hand, the locations of high stresses are more scattered, due to a smoother notch geometry. The specimens of test series 1 are cruciform joints, including four welds each. Since all welds are loaded equally, the area of possible crack initiation is about 40 cm long. Areas of high stress are scattered throughout the weld length. Due to the poor visibility of these stress peaks when displaying the entire weld, not much additional value is gained from stress plots of series one, which is why they are omitted in Fig. 3.

The fatigue hot spots of the specimens of series two and three are significantly smaller, as seen in Figs. 2 and 3. For those two series, the crack initiation site matches the location of the maximum stress in the FE calculation. In the first test series, however, the peak stress only predicts the correct location of crack initiation in roughly 60% of the cases, which is a further indicator of why considering nonlocal effects might lead to more accurate fatigue life predictions.

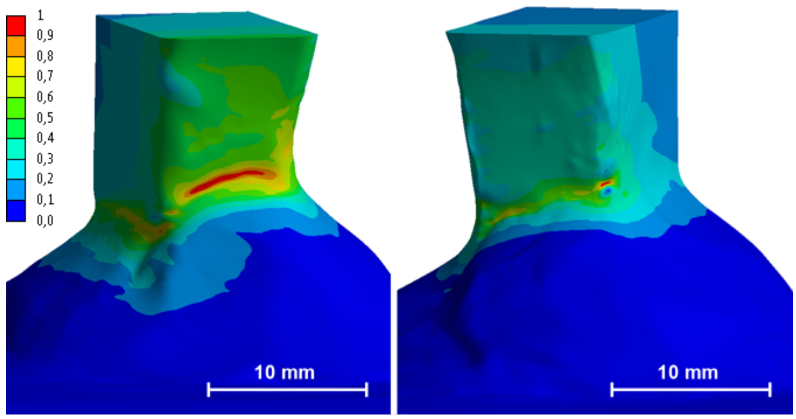

(a) Series 2

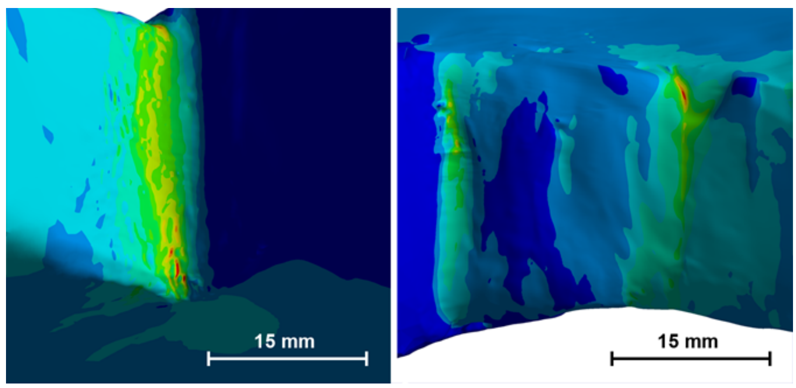

(b) Series 3

Fig. 3: Von Mises stress distribution at critical fatigue spots in specimens of series 2 and 3. Comparison between sharply and mildly notched specimens. Displayed stress values are normalized.

5.1 Scanning

The specimens are scanned using a 3D scanning device by the company FARO [49]. According to the manufacturer, the scans have a resolution of 50 μm and an accuracy of 25 μm with a statistical significance of twice the standard deviation. After removing outliers from the obtained point cloud, C1-continuous NURBS (Non-Uniform Rational B-Spline) surfaces are fitted to the scanned data. The C1-continuity is necessary to get convergent stress results in the following FEA. Subsequently, 3D solids are generated through Boolean operations and imported into ANSYS [50]. The advantages of incorporating 3D scans of the weld in the fatigue assessment is investigated by comparing fatigue life predictions to results obtained with an idealized weld form. Therefore, a weld flank angle of 45° and notch radii of 1 mm are assumed, as these values are frequently used in the literature, e.g., [8, 51–53].

5.2 Numerical Modeling

The imported solids are sliced into parts to apply different meshing options. Due to the small element sizes necessary to accurately capture the scanned weld geometries, which lead to a large number of elements, submodels are used. The mesh of the global model consists of 20-node tetrahedral elements with edge lengths of approximately 3 mm. In the submodel, the same element type is used with a base size of 1 mm. At the weld surface, curvature sizing is defined with an angle of 3° and a growth rate of 1.25. A curvature angle of 3° implies that 120 elements are used along the boundary of a circle. The edge size is automatically chosen according to the radius of that circle. By doing so, sharp notches are meshed in greater detail due to their smaller notch radii. A previous convergence study [48] confirmed that the chosen mesh settings yield convergent and accurate stress results. For test series 1, each of the four welds is assessed with an individual submodel as each one contains up to almost 1e7 elements, depending on the actual shape of the weld. The material law is set to linear elastic in both the global and the submodel. Obtained stress tensors are exported to CSV-files and post-processed with a Python script.

5.3 Post-Processing

The fatigue indicators described in section 2 are calculated at each element node. For the nonlocal and the probabilistic approach, the surface area and volume associated with each element node are also required. Dividing the element volume by the number of corner nodes in the regarded element yields the volume related to each element node. Similarly, the corresponding surface areas are calculated by dividing the area of an element face by the number of corner nodes on that surface. Due to the small element sizes (edge lengths of about 0.01 mm in the critical fatigue area) and the low shape distortions of the elements, the described determination of areas and volumes is considered sufficiently accurate.

In the local models, only the maximum values of the fatigue indicator parameters are used to predict fatigue lives. Therefore, the Wöhler curve is obtained in one step through minimizing the RSME with respect to fatigue life. The determination of the required parameters of the support factor approach, on the other hand, involves two steps per iteration. First, the parameter κ is chosen arbitrarily, so that the support factor n_{supp} of every specimen can be calculated. Secondly, the parameters $\mathcal{A}$ and $\mathcal{B}$ are determined through least-squares fitting. The applied trust-region algorithm varies the value of κ in order to obtain an overall minimum of the RMSE. Iteratively calculating the highly stressed regions of all specimens, which may contain up to 1e7 elements each, is costly and time-consuming. Therefore, element nodes with similar stress values are grouped into bins to reduce the computational effort. Surface areas or volumes of all nodes within the bin range are added to obtain the area or volume corresponding to that bin. The stress value is the area- or volume-weighted average of all nodes within the bin. In total, 100 bins are defined. Their widths grow with a rate of 5%, leading to narrower bins at high stresses. The first one has a width of approximately 0.04%, whereas the last one contains everything below 4.8% of the maximum stress value. By doing so, the sharp stress gradients at the notch are accurately captured.

The parameter-fitting of the probabilistic model uses the same binned data. One can derive the failure probability of a specimen by replacing the integral in Eq. (13) with the sum of all bins.

$$P_{\mathrm{f}} = 1 - \prod_{i}^{\#\mathrm{bins}} S_i = 1 - \exp\left(\text{-}z\lambda^{-\beta} \sum_{i}^{\#\mathrm{bins}} \left(\log_{10} n_{\mathrm{f}} - \theta_i\right)^{\beta} V_i \right) \tag{15}$$

Maximum Likelihood Estimation (MLE) [54] yields the parameters of the probabilistic model. The derivatives of Eq. (15) are determined analytically, but the obtained equations are solved numerically. For numerical reasons, the logarithm of the likelihood function is used. Owing to their monotonic properties, the maxima of the likelihood and the log-likelihood function occur at the same location.

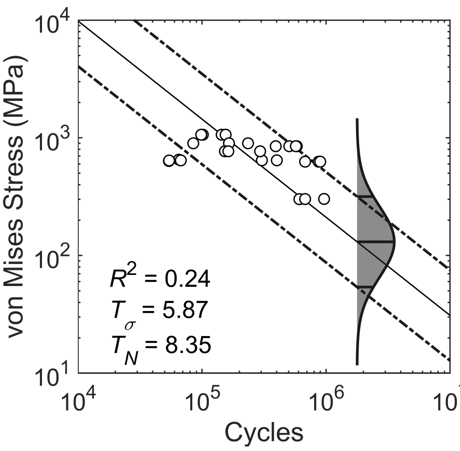

(a) Idealized weld geometry

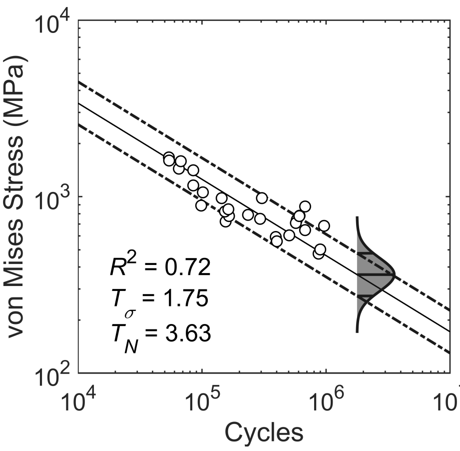

(b) Scanned weld geometry

Fig. 4: Resulting Wöhler curves using peak stress values. Comparison between (a) idealized and (b) scanned weld geometry. Dot-dashed lines indicate 10%- and 90%-quantiles.

6 Results and Discussion

6.1 Local Model

In a first step, fatigue lives are predicted from maximum stress values and compared to the experimental results of Section 5. The models are evaluated based on the R^2 metric of the fitted curve and its scatter range indices T_σ and T_N. The scatter range T_σ is defined as the quotient of the 10%- and 90%-quantiles of the stress values, which are also displayed in Fig. 4. T_N is determined analogously, using fatigue life instead of stress. For the idealized weld geometry, poor agreement between predicted and experimental fatigue lives is observed. The goodness of fit of the resulting Wöhler curve, which is described by the parameters $\mathcal{A}$ = -1.20 and $\mathcal{B}$ = 8.79, is only 0.24. Its scatter ranges are T_σ = 5.87 and T_N = 8.35 concerning peak stress and fatigue life, respectively. Including 3D scans of the weld into the assessment approach, increases the prediction accuracy of the local model significantly, as seen by comparing Fig. 4a to Fig. 4b. The peak stress model in combination with scanned weld geometries yields an R^2 value of 0.72, and scatter measures of $T_\sigma = 1.75$ and $T_N = 3.63$.

With regard to the investigated fatigue indicator parameters, Tab. 1 reveals that for the scanned geometries, the R^2 values of all models differ only marginally, ranging from 0.70 to 0.72. The scatter indices, on the other hand, confirm the signed von Mises stress, the maximum principal stress, the maximum shear stress, and the critical-plane damage parameter as the best indicators do predict fatigue life as their metrics are close to each other. The Fatemi-Socie damage parameter shows slightly worse results, and the strain energy density release rate, especially in combination with an idealized geometry, by far the worst ones.

6.2 Nonlocal Model

Since fatigue life is influenced not only by the maximum stress value but also by the stress field in the vicinity of the notch, taking into account the size of the highly stressed region around the notch may lead to more accurate predictions. In this work, the support factor approach presented in section 4 is used. The highly stressed region is defined once in terms of volume and once in terms of surface area.

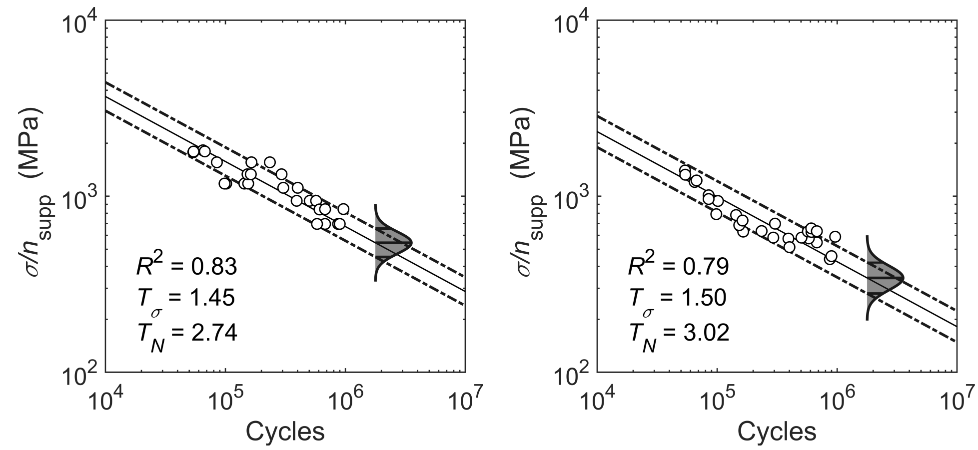

(a) Idealized weld geometry (b) Scanned weld geometry

Fig. 5: Wöhler curves obtained with the support factor approach incorporating the highly stressed surface area. Comparison between (a) idealized and (b) scanned weld geometry. Dot-dashed lines indicate 10%- and 90%-quantiles.

The peak stress values are corrected by the support factor according to Eq. (7), which corresponds to a shift in the log-log plot, and then used to fit the linear Wöhler curves. The results are displayed in Figs. 5 and 6. All four combinations of ideal versus scanned geometry and area versus volume yield to superior prediction accuracies compared to the previous, local model. However, the unexpected observation is that the nonlocal approach yields better results when applied to an idealized weld geometry instead of an exact representation of the weld. If the surface area is used to account for the highly stressed region,

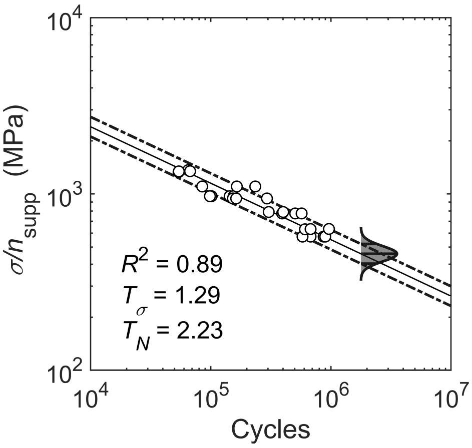

(a) Idealized weld geometry

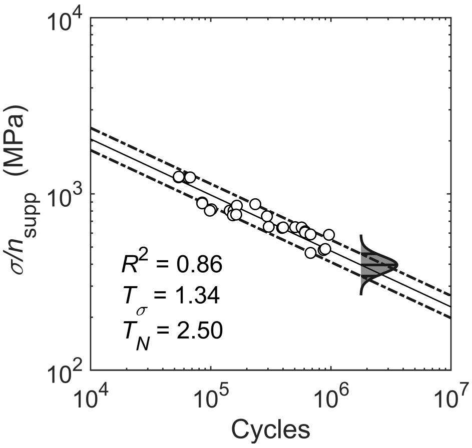

(b) Scanned weld geometry

Fig. 6: Wöhler curves obtained with the support factor approach incorporating the highly stressed volume. Comparison between (a) idealized and (b) scanned weld geometry. Dot-dashed lines indicate 10%- and 90%-quantiles.

the coefficients of determination are 0.83 and 0.79 for the idealized and scanned geometry, respectively. By using the volume instead, these values increase to $R^2 = 0.89$ (idealized) and $R^2 = 0.86$ (scanned). The scatter measures T_σ and T_N correlate with the presented R^2 values and are displayed in Figs. 5 and 6, or Tab. 1. Despite the great effort that is required to obtain a 3D representation of the weld through laser scanning, and the complexity added to the model, worse results are observed. Based on the available data of this contribution, one can, therefore, conclude that scanning welds is not worth its effort if nonlocal effects are considered. However, this statement may only be true for elastically determined fatigue indicator parameters. If plasticity is taken into account, the actual material behavior at the notch is captured more accurately, which might lead to superior prediction accuracies for the scanned geometries. The investigation of this hypothesis is not part of this paper, and has to be verfified in future works.

Another fact worth mentioning is that the presented R^2 values and scatter range indices of the nonlocal models indicate that the volume should be used to consider size effects instead of the surface area. A possible explanation as to why the volume is a better proxy to incorporate the highly stressed region is the fact that by doing so, stress gradients perpendicular to the surface, which are said to influence fatigue life, are taken into account.

Similar to the local model, the maximum principal stress, the maximum shear stress, and the critical-plane damage parameter are equally well suited for fatigue life predictions. The signed von Mises stress is able to explain slightly more experimental scatter, as seen in Tab. 1. The Fatemi-Socie parameter shows worse evaluation statistics compared to the previously mentioned indicators. However, one should keep in mind that the investigated specimens were subjected to constant amplitude loading, but the Fatemi-Socie parameter is usually applied to multiaxial fatigue problems due to its ability to account for nonproportional loading. The strain energy density release rate is the overall worst parameter for

	Method		$\mathcal{A}$	$\mathcal{B}$	κ	T_X	T_N	R^2
σ_Σ	Local	i	-1.20	8.79	-	5.87	8.35	0.24
		s	-2.32	12.18	-	1.75	3.63	0.72
	Area	i	-2.71	13.66	5.28	1.45	2.74	0.83
		s	-2.71	13.12	19.3	1.50	3.02	0.79
	Volume	i	-3.12	14.56	5.75	1.29	2.23	0.89
		s	-3.15	14.43	7.00	1.34	2.50	0.86
σ_1	Local	i	-1.21	8.86	-	5.77	8.35	0.24
		s	-2.26	12.10	-	1.80	3.75	0.70
	Area	i	-2.96	15.64	2.83	1.35	2.41	0.87
		s	-2.65	13.05	18.6	1.54	3.14	0.78
	Volume	i	-3.06	15.11	4.21	1.32	2.36	0.88
		s	-2.93	13.55	16.9	1.42	2.79	0.82
$\tau_{\max}$	Local	i	-1.21	8.50	-	5.76	8.34	0.24
		s	-2.27	11.45	-	1.79	3.74	0.71
	Area	i	-2.94	14.55	2.96	1.35	2.43	0.87
		s	-2.66	12.28	19.1	1.53	3.12	0.78
	Volume	i	-3.11	14.12	4.45	1.31	2.29	0.88
		s	-3.12	13.50	6.94	1.34	2.50	0.86
P_{CP}	Local	i	-1.07	2.91	-	7.65	8.80	0.20
		s	-2.39	0.09	-	1.73	3.70	0.71
	Area	i	-3.13	-0.16	2.98	1.29	2.23	0.89
		s	-2.75	-0.92	19.9	1.53	3.20	0.77
	Volume	i	-3.15	-0.61	3.71	1.30	2.29	0.88
		s	-2.98	-1.78	18.2	1.43	2.94	0.80
P_{FS}	Local	i	-0.86	3.24	-	12.3	8.56	0.22
		s	-1.43	2.34	-	2.49	3.69	0.71
	Area	i	-2.22	2.67	1.63	1.76	3.52	0.73
		s	-1.68	1.60	12.3	1.98	3.16	0.78
	Volume	i	-2.31	0.60	3.34	1.72	3.47	0.74
		s	-1.88	0.82	10.9	1.75	2.87	0.81
Y	Local	i	-0.31	5.35	-	1441	9.70	0.13
		s	-1.17	6.24	-	3.13	3.80	0.70
	Area	i	-0.41	6.29	0.91	183	8.33	0.24
		s	-1.34	6.17	9.99	2.45	3.33	0.76
	Volume	i	-0.38	5.59	2.06	278	8.57	0.22
		s	-1.48	5.91	8.59	2.12	3.03	0.79

Tab. 1: Parameters and statistics of the local and nonlocal models. The abbrevations (i) and (s) indicate models with idealized and scanned geometries, respectively.

predicting fatigue life. Especially if combined with idealized weld geometries, extremely poor results are obtained.

6.3 Probabilistic Model

Plotting fatigue life curves, similar to the previous two models (Figs. 4, 5, and 6), is no longer possible. Since specimens from different experimental series are investigated, no common scalar value can be displayed on the y-axis. The Weibull models are, therefore, evaluated based on two different characteristics. On the one hand, fatigue lives corresponding to a survival probability of 50% are estimated and compared to the ones observed in the experiments, as shown in Fig. 7. From those values, Pearson's coefficient of correlation R and the scatter range index with respect to fatigue life T_N is determined. Additionally, an artificial standard deviation based on the four model parameters ($\mathcal{A}$, $\mathcal{B}$, λ, and β) and the actual stress distribution of each specimen is introduced. For every specimen, fatigue lives for n equidistantly distributed failure probabilities are calculated, as illustrated in Fig. 8. Afterward, the determined fatigue lives are shifted along the x-axis, aligning the location of the median of each specimen. The standard deviation (on a logarithmic scale) is then calculated from all the previously estimated fatigue lives. The number of fatigue lives necessary to obtain a sufficient precision was determined through a preceding convergence study and resulted in $n = 1000$. The obtained evaluation metrics of all probabilistic models are shown in Tab. 2.

Similarily to the nonlocal approach, the idealized weld geometry leads to more accurate models with respect to both the standard deviation and comparing predicted cycles (50% survival probability) to experimentally determined ones. Concerning the integral in Eq. (13), defining the weakest link model in terms of the specimen's volume instead of its surface area yields superior results as well. The combination of an idealized weld geometry and using the volume integral, therefore, results in the most accurate predictions with a standard deviation of 0.22 for the investigated specimens and the signed von Mises equivalent stress. The coefficient of correlation of the predicted and observed fatigue lives is $R = 0.942$, and the scatter amounts to $T_N = 2.38$.

Regarding the investigated fatigue indicator parameters, it is seen that the prediction accuracies are of almost equal quality, with the signed von Mises stress leading to marginally better results overall. In contrast to the observations for the local and nonlocal models, the strain energy density release rate yields similar standard deviations and R values as the other five fatigue indicator parameters. However, if applied to idealized weld geometries, it is not able to accurately predict fatigue behavior.

It is further investigated how much each subvolume contributes to the overall failure probability of the specimen. In other words, it is determined whether the failure probability is governed by the maximum stress value or by regions subjected to lower stresses. Therefore, the stress values and volumes associated with each element node are divided into 100 equidistant bins. Each bin represents a stress range of 1%, which means that the first bin contains all element nodes with stresses between 99% and 100% of the maximum stress value. The volumes associated with each element node are added to obtain the volume of the bin. The stress value associated with the bin is the volume-weighted average of all nodes in the bin.

The failure probabilities are then calculated separately for every bin, according to Eq. (15). Figure 9 displays the failure probabilities of every specimen, as well as the median among all specimens. Figure 9a shows that for the idealized weld geometry, the contributing region ranges from around 20% to almost 100% of the maximum stress value, with a peak at about 30%. For the scanned weld geometries, on the

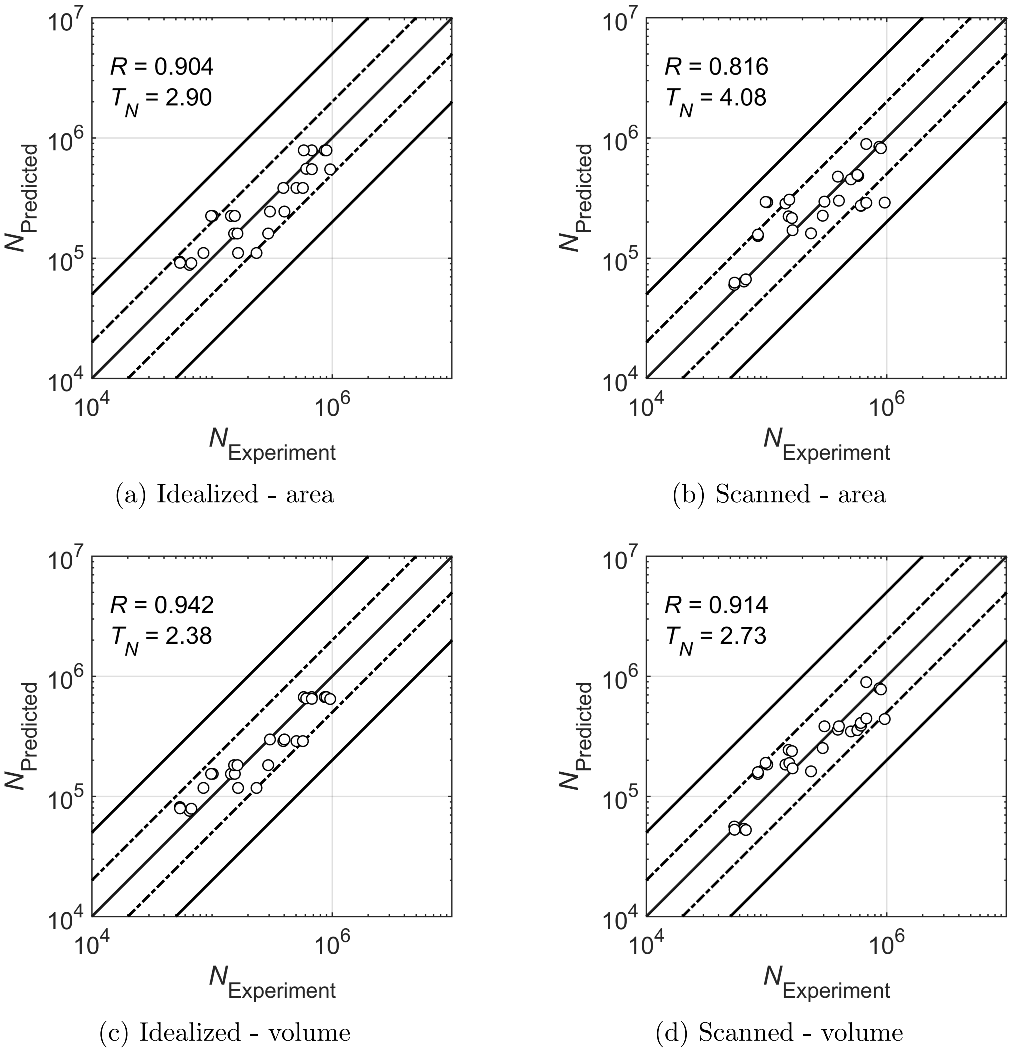

Fig. 7: Weibull model predictions for a survival probability of 50% versus observed cycles in the experiments. All combinations of weld geometry and highly stressed region are displayed. The black dot-dashed and the full line represent a deviation factor of 2 and 5, respectively.

other hand, the contributing region is narrower and shifted more towards the lower stress values (approximately 10% to 60% of the maximum stress). The accurate representation of the weld geometry results in steep stress gradients at the notch, which means that the volume associated with the maximum stress is small. The failure probability of this peak stress is high, but since it is scaled with the corresponding subvolume, the failure probability of the specimen is hardly affected, as seen in Fig. 9b.

On the contrary, the failure probabilities of the lower stress ranges are lower, but the associated volumes are significantly larger, leading to greater contributions to the overall failure probability of the specimen. One can also deduce from Fig. 9 that the contributing stress ranges vary from specimen to specimen. Whereas low stresses (relative to the maximum stress value) contribute the most to the overall failure probability for sharply notched specimens (due to the high stress concentration and peak stresses), the contributing stress ranges are closer to the peak stress value for mild notches. For both the idealized and

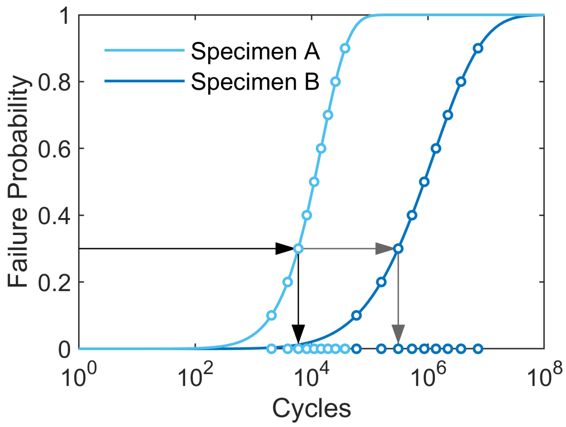

Fig. 8: Schematic representation of determining the standard deviation of the Weibull model for each specimen.

the scanned weld geometry, the contribution of the maximum stress value to the failure probability is insignificant. This observation might additionally support the hypothesis that nonlocal effects should be considered in fatigue assessment approaches.

7 Conclusions

The contribution at hand investigated the advantages of using laser-scanned welds over idealized weld geometries in fatigue life estimations. A total of 60 fatigue models, including six different fatigue indicator parameters, derived from elastically calculated stress tensors, were fitted to experimental results from three test series, and their abilities to accurately predict fatigue lives was assessed. Based on the results and discussion presented, the following conclusions can be drawn.

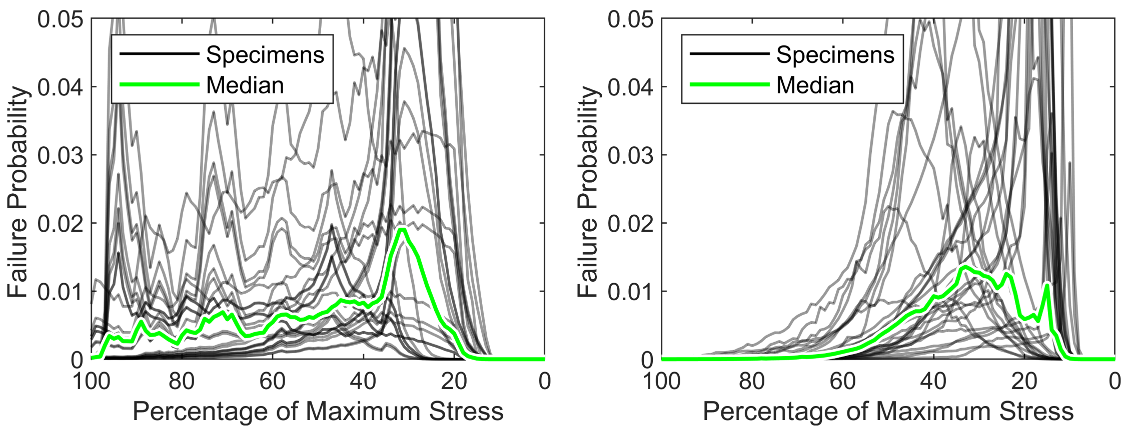

(a) Idealized weld geometry (b) Scanned weld geometry

Fig. 9: Individual contribution according to Eq. (15) of 100 equidistant stress bins (1% stress range each) to the overall failure probability of the specimens. Graphs are shown at the example of the Weibull model using the volume integral in combination with (a) idealized and (b) scanned weld geometries.

	Method		$\mathcal{A}$	$\mathcal{B}$	λ	β	std	T_N	R
σ_Σ	Area	i	-2.38	12.64	5.51	26.0	0.22	2.90	0.90
		s	-2.04	12.48	6.06	15.7	0.29	4.08	0.82
	Volume	i	-2.79	13.64	3.51	10.9	0.22	2.38	0.94
		s	-2.81	13.87	4.91	16.3	0.22	2.73	0.91
σ_1	Area	i	-2.19	12.24	5.63	23.9	0.24	3.13	0.90
		s	-1.88	12.45	5.35	10.8	0.30	4.40	0.79
	Volume	i	-2.71	14.33	3.61	5.29	0.23	2.58	0.93
		s	-2.72	13.85	5.07	15.6	0.23	2.84	0.91
$\tau_{\max}$	Area	i	-2.19	11.59	5.62	24.0	0.24	3.12	0.90
		s	-1.92	11.97	5.24	10.5	0.29	4.34	0.80
	Volume	i	-2.68	13.40	4.04	6.83	0.24	2.59	0.93
		s	-2.79	13.06	4.90	15.7	0.22	2.71	0.92
P_{CP}	Area	i	-2.25	0.74	5.48	23.1	0.24	3.06	0.91
		s	-1.94	2.27	6.18	15.4	0.30	4.05	0.82
	Volume	i	-2.67	-0.33	4.40	14.0	0.24	2.79	0.92
		s	-2.68	-0.07	5.25	15.4	0.23	2.71	0.92
P_{FS}	Area	i	-1.62	3.23	4.19	5.49	0.30	4.23	0.82
		s	-1.48	3.25	5.85	15.1	0.29	4.08	0.82
	Volume	i	-2.78	68.2	95.7	1.28	0.28	2.87	0.90
		s	-2.16	0.78	4.49	14.2	0.22	2.74	0.91
Y	Area	i	-0.54	138	181	1.23	0.38	8.75	0.48
		s	-0.92	7.35	6.19	14.9	0.30	4.21	0.81
	Volume	i	-0.37	8.98	8.98	15.4	0.36	9.04	0.45
		s	-1.24	6.92	5.45	15.3	0.24	2.88	0.91

Tab. 2: Parameters and statistics of the probabilistic models. The abbrevations (i) and (s) indicate models with idealized and scanned geometries, respectively.

- Using an idealized weld geometry in combination with the local model, namely solely focusing on the maximum fatigue indicator parameter, led to extremely poor fatigue life predictions, as seen in Fig. 4a and Tab. 1. Fig. 4b shows that incorporating 3D scans of the weld root in the assessment process, improved the prediction accuracy of the model significantly. For the von Mises equivalent stress, the R^2 value of the fitted Wöhler curve was increased from 0.24 to 0.72.

- Even better results were obtained by incorporating nonlocal effects, i.e., through a support factor calculated from the highly stressed volume or area. Interestingly, the combination of idealized weld geometry and the nonlocal approach was able to predict fatigue lives more accurately compared to using scanned weld geometries in combination with both the local model and the nonlocal model. The difference between the R^2 values was not significant, namely 0.83 to 0.79 and 0.89 to 0.86 for the area and volume approach, respectively, but still evident. This implies that scanning welds is not only costly but also decreases the prediction accuracy of the model. However, this was only confirmed for linear elastic calculations. Incorporating plasticity might improve the quality of fatigue predictions from scanned weld geometries and is prospect of further research.

- For both the support factor approach and the Weibull model, the volume was a better proxy to account for the highly stressed region of the component (compared to the surface area), as seen in Figs. 5, 6, and 7. This circumstance may be explained by the fact that gradient effects perpendicular to the specimen's surface are taken into account if the volume is used.
- In the probabilistic model, the maximum stress value contributed little towards the failure probability of the specimen as seen in Fig. 9. Due to the high stress gradients at the notch, the region associated with the maximum stress value is extremely small, especially for the scanned weld geometry. This might also be an indicator against the use of local approaches in fatigue assessment.
- All the investigated fatigue indicators, except for the strain energy density release rate, showed similar results with the signed von Mises stress leading to slightly better prediction accuracies overall. This is not surprising since the experiments were conducted under constant amplitude loading. However, different results, especially for the critical-plane approach and the Fatemi-Socie parameter, are to be expected for nonproportional loading and multiaxial fatigue.

8 Acknowledgment

I would like to thank the Marshall Plan Foundation for funding my research visit through the Marshallplan scholarship. Without their financial support, the collaboration would not have been possible in this way. Additionally, I am grateful to Prof. Derek Warner for his great supervision during my stay at Cornell and his warmhearted hospitality. Last but not least, I want to thank Prof. Gerhard Lener, who fully supported my plans of going abroad to collaborate with the Cornell Fracture Group and also supervised my research. Thank you all for this great experience.

9 References

[1] N. J. Delatte. *Beyond failure: Forensic case studies for civil engineers*. Reston, Va.: American Society of Civil Engineers, 2009.

[2] J. F. Lancaster. *Engineering catastrophes: Causes and effects of major accidents*. 3rd ed. Woodhead Publishing in materials. Cambridge and Boca Raton, FL: Woodhead, 2005.

[3] A. Brot. "Development of Fatigue Life Regulations Based on Lessons Learned from Several Aircraft Accidents". In: *Israel Annual Conference on Aerospace Sciences 2016* (2016).

[4] C. Berger, B. Pyttel, and D. Schwerdt. "Beyond HCF - Is there a fatigue limit?" In: *Materialwissenschaft und Werkstofftechnik* 39.10 (2008), pp. 769–776.

[5] B. Pyttel, D. Schwerdt, and C. Berger. "Very high cycle fatigue – Is there a fatigue limit?" In: *International Journal of Fatigue* 33.1 (2011), pp. 49–58.

[6] P. Chowdhury and H. Sehitoglu. "Mechanisms of fatigue crack growth - a critical digest of theoretical developments". In: *Fatigue & Fracture of Engineering Materials & Structures* 39.6 (2016), pp. 652–674.

[7] Austrian Standards Institute. *Eurocode 3: Design of steel structures. Part 1-9: Fatigue*. 2013.

[8] A. F. Hobbacher. *Recommendations for Fatigue Design of Welded Joints and Components*. 2nd ed. 2016. IIW Collection. Cham: Springer International Publishing, 2016.

[9] R. Rennert, E. Kullig, M. Vormwald, A. Esderts, and D. Siegele. *Rechnerischer Festigkeitsnachweis für Maschinenbauteile: Aus Stahl, Eisenguss- und Aluminiumwerkstoffen*. 6. FKM-Richtlinie. VDMA, 2012.

[10] W. Fricke, A. Kahl, and H. Paetzold. "Fatigue Assessment of Root Cracking of Fillet Welds Subject to Throat Bending using the Structural Stress Approach". In: *Welding in the World* 50.7-8 (2006), pp. 64–74.

[11] H. Neuber. "Über die Berücksichtigung der Spannungskonzentration bei Festigkeitsberechnungen". In: *Konstruktion* 20.7 (1968), pp. 245–251.

[12] A. Niederwanger, D. H. Warner, and G. Lener. "The Benefits of 3D Laser Scanning in the Fatigue Assessment of Welded Joints". In: *submitted to International Journal of Fatigue* (2020).

[13] H. Pang. "Analysis of weld toe profiles and weld toe cracks". In: *International Journal of Fatigue* 15.1 (1993), pp. 31–36.

[14] M. M. Alam, Z. Barsoum, P. Jonsén, A. Kaplan, and H. Häggblad. "The influence of surface geometry and topography on the fatigue cracking behaviour of laser hybrid welded eccentric fillet joints". In: *Applied Surface Science* 256.6 (2010), pp. 1936–1945.

[15] E. Lang, J. Rudolph, H. T. Beier, and M. Vormwald. "Geometrical Influence of a Butt Weld in the Low Cycle Fatigue Regime". In: *Procedia Engineering* 66 (2013), pp. 73–78.

[16] S. Liinalampi, H. Remes, and J. Romanoff. "Influence of three-dimensional weld undercut geometry on fatigue-effective stress". In: *Welding in the World* 87 (2018), p. 143.

[17] B. Schork, P. Kucharczyk, M. Madia, U. Zerbst, J. Hensel, J. Bernhard, Tchuindjang, M. Kaffenberger, and M. Oechsner. "The effect of the local and global weld geometry as well as material defects on crack initiation and fatigue strength". In: *Engineering Fracture Mechanics* 198 (2018), pp. 103–122.

[18] C.-Y. Hou. "Fatigue analysis of welded joints with the aid of real three-dimensional weld toe geometry". In: *International Journal of Fatigue* 29.4 (2007), pp. 772–785.

[19] M. Kaffenberger and M. Vormwald. "Fatigue resistance of weld ends - Analysis of the notch stress using real geometry". In: *Materialwissenschaft und Werkstofftechnik* 42.10 (2011), pp. 874–880.

[20] M. Kaffenberger and M. Vormwald. "Application of the notch stress concept to the real geometry of weld endpoints". In: *Materialwissenschaft und Werkstofftechnik* 42.4 (2011), pp. 289–297.

[21] E. Lang, J. Rudolph, T. Beier, and M. Vormwald. "Low Cycle Fatigue Behavior of Welded Components: A New Approach — Experiments and Numerical Simulation". In: *ASME 2012 Pressure Vessels and Piping Conference*. American Society of Mechanical Engineers Digital Collection, 2012, pp. 289–298.

[22] A. Bosch, E. Lang, and M. Vormwald. "Low Cycle Fatigue of Seam Welds – Numerical Simulation under Consideration of Material Inhomogeneities". In: *Procedia Engineering* 74 (2014), pp. 218–227.

[23] P. Stasiuk, A. Karolczuk, and W. Kuczko. "Analysis of Correlation between Stresses and Fatigue Lives of Welded Steel Specimens Based on Real Three-Dimensional Weld Geometry". In: *Acta Mechanica et Automatica* 10.1 (2016), pp. 12–16.

[24] R. Lang, G. Lener, J. Schmid, and M. Ladinek. "Schweißnahtbewertung basierend auf 3D-Laserscanning: Praktische Anwendung eines mobilen Laserscansystems zur Oberflächenbewertung von Schweißnähten - Teil 1". In: *Stahlbau* 85.5 (2016), pp. 336–343.

[25] R. Lang and G. Lener. "Schweißnahtbewertung basierend auf 3D-Laserscanning: Praktische Anwendung eines mobilen Laserscansystems zur Oberflächenbewertung von Schweißnähten - Teil 2". In: *Stahlbau* 85.6 (2016), pp. 395–408.

[26] R. Lang and G. Lener. "Application and comparison of deterministic and stochastic methods for the evaluation of welded components' fatigue lifetime based on real notch stresses". In: *International Journal of Fatigue* 93 (2016), pp. 184–193.

[27] S. Liinalampi, H. Remes, P. Lehto, I. Lillemäe, J. Romanoff, and D. Porter. "Fatigue strength analysis of laser-hybrid welds in thin plate considering weld geometry in microscale". In: *International Journal of Fatigue* 87 (2016), pp. 143–152.

[28] M. Ladinek, A. Niederwanger, R. Lang, J. Schmid, R. Timmers, and G. Lener. "The strain-life approach applied to welded joints: Considering the real weld geometry". In: *Journal of Constructional Steel Research* 148 (2018), pp. 180–188.

[29] M. Ladinek, A. Niederwanger, and R. Lang. "An individual fatigue assessment approach considering real notch strains and local hardness applied to welded joints". In: *Journal of Constructional Steel Research* 148 (2018), pp. 314–325.

[30] T. Stenberg, E. Lindgren, and Z. Barsoum. "Development of an algorithm for quality inspection of welded structures". In: *Proceedings of the Institution of Mechanical Engineers, Part B: Journal of Engineering Manufacture* 226.6 (2012), pp. 1033–1041.

[31] T. Stenberg, Z. Barsoum, E. Åstrand, A. . E. Öberg, C. Schneider, and J. Hedegård. "Quality control and assurance in fabrication of welded structures subjected to fatigue loading". In: *Welding in the World* 61.5 (2017), pp. 1003–1015.

[32] T. Stenberg, Z. Barsoum, J. Hedlund, and J. Josefsson. "Development of a computational fatigue model for evaluation of weld quality". In: *Welding in the World* (2019).

[33] S. Chaudhuri, J. Crump, P. A. S. Reed, and B. G. Mellor. "High-resolution 3D weld toe stress analysis and ACPD method for weld toe fatigue crack initiation". In: *Welding in the World* 63.6 (2019), pp. 1787–1800.

[34] W. N. Findley. "A Theory for the Effect of Mean Stress on Fatigue of Metals Under Combined Torsion and Axial Load or Bending". In: *Journal of Manufacturing Science and Engineering* 81.4 (1959), pp. 301–305.

[35] A. Karolczuk and E. Macha. "A Review of Critical Plane Orientations in Multiaxial Fatigue Failure Criteria of Metallic Materials". In: *International Journal of Fracture* 134.3 (2005), p. 267.

[36] A. Fatemi and D. F. Socie. "A Critical Plane Approach to Multiaxial Fatigue Damage Including Out-of-Phase Loading". In: *Fatigue & Fracture of Engineering Materials and Structures* 11.3 (1988), pp. 149–165.

[37] R. I. Stephens, A. Fatemi, R. R. Stephens, and H. O. Fuchs. *Metal fatigue in engineering*. 2nd ed. A Wiley-interscience publication. New York: Wiley, 2001.

[38] J. Lemaitre. *A Course on Damage Mechanics*. Berlin, Heidelberg: Springer Berlin Heidelberg, 1992.

[39] R. Kuguel. "A relation between theoretical stress concentration factor and fatigue notch factor deduced from the concept of highly stressed volume". In: *ASTM Proc.* 61 (1961), pp. 732–748.

[40] M. Kaffenberger and M. Vormwald. "Considering size effects in the notch stress concept for fatigue assessment of welded joints". In: *Computational Materials Science* 64 (2012), pp. 71–78.

[41] R. Wang, D. Li, D. Hu, F. Meng, H. Liu, and Q. Ma. "A combined critical distance and highly-stressed-volume model to evaluate the statistical size effect of the stress concentrator on low cycle fatigue of TA19 plate". In: *International Journal of Fatigue* 95 (2017), pp. 8–17.

[42] C. M. Sonsino and G. Fischer. "Local Assessment Concepts for the Structural Durability of Complex Loaded Components". In: *Materialwissenschaft und Werkstofftechnik* 36.11 (2005), pp. 632–641.

[43] T. Bruder, K. Störzel, and J. Baumgartner. "Fatigue assessment of seam welds of automotive components by local stress approaches". In: *Materialwissenschaft und Werkstofftechnik* 39.10 (2008), pp. 726–733.

[44] C.-K. Lin and W.-J. Lee. "Effects of highly stressed volume on fatigue strength of austempered ductile irons". In: *International Journal of Fatigue* 20.4 (1998), pp. 301–307.

[45] J. Liu and H. Zenner. "Fatigue Limit and Geometrical and Statistical Size Effect (in German)". In: *Materialwissenschaft und Werkstofftechnik* 22.6 (1991), pp. 187–196.

[46] P. Li, D. H. Warner, and N. Phan. "Predicting the Fatigue Performance of an Additively Manufactured Ti-6Al-4V Component from Witness Coupon Behavior". In: *submitted to International Journal of Fatigue* (2020).

[47] W. Weibull. "A Statistical Distribution Function Of Wide Applicability". In: *Journal of Applied Mechanics* 18 (1951), pp. 293–297.

[48] A. Niederwanger, M. Ladinek, and G. Lener. "Strain-life fatigue assessment of scanned weld geometries considering notch effects". In: *Engineering Structures* 201 (2019), p. 109774.

[49] FARO. *Edge and Laser Line Probe.*

[50] ANSYS Inc. *Ansys 2019 R1.* 2019.

[51] C. M. Sonsino. "A Consideration of Allowable Equivalent Stresses for Fatigue Design of Welded Joints According to the Notch Stress Concept with the Reference Radii rref = 1.00 and 0.05 mm". In: *Welding in the World* 53.3 (2009), R64–R75.

[52] K. Saiprasertkit, T. Hanji, and C. Miki. "Fatigue strength assessment of load-carrying cruciform joints with material mismatching in low- and high-cycle fatigue regions based on the effective notch concept". In: *International Journal of Fatigue* 40 (2012), pp. 120–128.

[53] J. Schijve. "Fatigue predictions of welded joints and the effective notch stress concept". In: *International Journal of Fatigue* 45 (2012), pp. 31–38.

[54] J. Aldrich. "R. A. Fisher and the making of maximum likelihood 1912-1922". In: *Statistical Science* 12.3 (1997), pp. 162–176.